

## Synthesis of $\beta$ -strontium hydrogen phosphate nanosheets and its effect on thermal and tribo-mechanical properties of polypropylene composites

Lemiye Atabek Savaş

Online Publication Date: 10 June 2022

URL: <http://www.jresm.org/archive/resm2022.404ma0810.html>

DOI: <http://dx.doi.org/10.17515/resm2022.404ma0810>

Journal Abbreviation: *Res. Eng. Struct. Mater.*

### To cite this article

Savas LA. Synthesis of  $\beta$ -strontium hydrogen phosphate nanosheets and its effect on thermal and tribo-mechanical properties of polypropylene composites. *Res. Eng. Struct. Mater.*, 2022; 8(4): 643-658.

### Disclaimer

All the opinions and statements expressed in the papers are on the responsibility of author(s) and are not to be regarded as those of the journal of Research on Engineering Structures and Materials (RESM) organization or related parties. The publishers make no warranty, explicit or implied, or make any representation with respect to the contents of any article will be complete or accurate or up to date. The accuracy of any instructions, equations, or other information should be independently verified. The publisher and related parties shall not be liable for any loss, actions, claims, proceedings, demand or costs or damages whatsoever or howsoever caused arising directly or indirectly in connection with use of the information given in the journal or related means.



Published articles are freely available to users under the terms of Creative Commons Attribution - NonCommercial 4.0 International Public License, as currently displayed at [here](https://creativecommons.org/licenses/by-nc/4.0/) (the "CC BY - NC").



Research Article

## Synthesis of $\beta$ -strontium hydrogen phosphate nanosheets and its effect on thermal and tribo-mechanical properties of polypropylene composites

Lemiye Atabek Savaş<sup>\*,a</sup>

Department of Materials Science and Engineering, Erciyes University, Kayseri, Turkey

### Article Info

### Abstract

#### Article history:

Received 22 Feb 2022

Revised 9 May 2022

Accepted 5 June 2022

#### Keywords:

Strontium hydrogen phosphate;  
Nanosheet;  
Polypropylene;  
Mechanical properties;  
Wear

$\beta$ -strontium hydrogen phosphate nanosheets (SHPs) with a thickness range of 35-50 nm were synthesized by hydrothermal method using strontium nitrate ( $\text{Sr}(\text{NO}_3)_2$ ) and diammonium hydrogen phosphate ( $(\text{NH}_4)_2\text{HPO}_4$ ) as reagents. Polypropylene (PP)/SHP nanocomposites were prepared using melt blending technique with different filler concentrations ranging from 1 wt.% to 7 wt.%. Composites were characterized primarily by tensile test, flexural test, thermogravimetric analyses and ball-on-disc sliding wear test. Experimental results revealed that the inclusion of nanosheets into PP improved the thermal stability of the composites. In addition, the tensile and flexural properties of the composites improved with SHP loading. A maximum increment of 6.0 % in tensile strength compared to pure PP was observed at 7 wt.% SHP concentration, and flexural strength of the composites was found to be higher than that of the pure polymer at each filler concentration. However, an increase was observed in the friction coefficient and wear rates of the composites due to increased hardness and rigidity of the matrix with the addition of SHP, which produced micro-cutting and micro-plowing actions that caused increased abrasive wear of the composites.

© 2022 MIM Research Group. All rights reserved

## 1. Introduction

In today's industry where specific strength is important along with advanced material properties, polymer composites have drawn significant attention with their high strength, light weight, good corrosion and chemical resistance properties compared to traditional engineering materials. In order to endow polymer composites with mechanical and functional properties, many kinds of micro- and nano-fillers can be added into the polymers [1, 2]. The micro-fillers usually require high volume fractions to have a significant influence on the properties of the composites [3]. However, high filler loadings may cause processing difficulties due to increased viscosity of the matrix material [1]. On the other hand, the incorporation of nano-fillers in very small amounts give the same or more contribution to the composites due to enhanced surface area and thus complex physical interactions between the reinforcement and the polymer matrix [1, 4, 5]. Furthermore, apart from mechanical improvements, thermal and functional characteristics obtained with nano-fillers make polymer nanocomposites unique candidates for specific industrial applications [6-8].

Nano-fillers can be classified according to their dimensional morphology as one dimensional (1D), two dimensional (2D), and three dimensional (3D), which all have their own advantages, disadvantages, and exclusive properties [1, 4]. The morphology of the nano-fillers plays an important role in the final nanocomposite performance [9]. It is well

\*Corresponding author: [atabekl@erciyes.edu.tr](mailto:atabekl@erciyes.edu.tr)

<sup>a</sup> [orcid.org/0000-0002-6504-5846](https://orcid.org/0000-0002-6504-5846)

DOI: <http://dx.doi.org/10.17515/resm2022.404ma0810>

Res. Eng. Struct. Mat. Vol. 8 Iss. 4 (2022) 643-658

known that the use of two dimensional (2D) nanofillers (sheets, platelets, or flakes) with high aspect ratio, significantly improves the thermal stability, mechanical and tribological properties of the composites [10, 11]. Since 2D nanofillers offer more contact area with polymer chains than 1D nanofillers, they show higher performance and are therefore more preferred in nanocomposites [12]. The previous studies revealed that good improvements in tensile strength, wear resistance and thermal stability of different polymers were obtained using 2D nanofillers in the structure such as graphene [12, 13], layered silicates [4, 14], layered double hydroxide [3, 15], hexagonal boron nitride [16], molybdenum disulfide [17, 18],  $\alpha$ -zirconium phosphate [19, 20], and layered metal carbides [11, 21]. Feng et al. [22] have reported that the addition of 1.6 wt.% molybdenum disulfide ( $\text{MoS}_2$ ) led to remarkably improved thermal stability of PP. In another work, Lonkar et al. [15] have demonstrated that organomodified layered double hydroxide (LDH) is highly effective at enhancing the elastic modulus and tensile strength of PP. They found that tensile strength and modulus of PP/LDH composite with 7 wt.% filler concentration was about 27% and 26% higher than pure PP, respectively. Sun et al. [19] have successfully synthesized  $\alpha$ -zirconium phosphate (ZrP) nanoplatelets through a hydrothermal method and then used it to improve the mechanical and tribological performance of polyamide 66 (PA66). Compared to pure PA66, they achieved 10% improvement in tensile modulus and 14% increase in tensile strength in the nanocomposite with 1.0 wt.% ZrP nanoplatelet content. At this concentration, 43% reduction in the coefficient of friction and 59% reduction in the wear rate of the composites was observed. In the light of these studies, it has been well recognized that different nanoplatelet additives may have positive results on the mechanical and tribological properties of polymer nanocomposites because of their high aspect ratio, high specific surface area and thin laminated structure. As with other synthetic 2D nanofillers, SHP nanosheets are also likely to have positive effects on the thermal, mechanical and wear resistance properties of PP.

In this study, considering the above mentioned advantageous nanosheet structure, the possible contribution of SHP on the tribo-mechanical and thermal properties of PP composites were investigated. When the literature is searched, it is realized that there are a limited number of studies on SHPs. These studies cover X-ray diffraction (XRD) analysis of different strontium phosphate compound powders including  $\alpha$ - and  $\beta$ - type for their value in the identification of phosphate materials [23], synthesis of  $\beta$ -type strontium hydrogen phosphate ( $\beta$ - $\text{SrHPO}_4$ ) nanosheets for using immobilization of lead ions from acidic aqueous solution [24], preparation of  $\alpha$ - and  $\beta$ - $\text{SrHPO}_4$  nanoparticles via a polyol-mediated synthesis and their characterization using XRD and Fourier transform infrared spectroscopy (FTIR) [25], and lastly the synthesis of  $\beta$ - $\text{SrHPO}_4$  and determining the range of incorporation of calcium into the structure for biomedical applications [26]. Apart from above mentioned works, no study has been found in which SHPs are combined with a polymer matrix and their structural and mechanical properties are examined.

PP matrix was selected in current study because of its advantageous properties such as being suitable for melt-based production methods, chemical and dimensional stability, affordable cost, high wear resistance, and its recent applications with several nanofillers such as graphene, montmorillonite, layered double hydroxide, and carbon nanotubes [27, 28]. Firstly, SHPs were successfully synthesized by a hydrothermal process and then blended with PP using melt blending via a twin screw extruder. Maleic anhydride-grafted polypropylene (MAPP) was used as compatibilizer to enhance interfacial adhesion of the constituents one step further. The characterization of SHPs has been carried out through XRD, field emission scanning electron microscopy (FE-SEM), FTIR, and thermogravimetric analysis (TGA). The effect of SHPs on the mechanical properties of PP was determined using tensile, flexural and Shore D hardness tests. The thermal and tribological properties of the composites were evaluated by using TGA and ball-on disc wear test, respectively.

After all, failure modes and wear mechanisms of the samples were analyzed and explicated. This work puts forth an opinion, for the first time, about the thermal, mechanical and wear performance contribution of SHP within a polymeric matrix. Throughout the study, the main advantages and limitations of the composites have been highlighted with the hope that this will pave the way for further works on different properties of SHP reinforced composites.

## 2. Materials and Methods

### 2.1. Materials

Diammonium hydrogen phosphate ((NH<sub>4</sub>)<sub>2</sub>HPO<sub>4</sub>) and cetyltrimethylammonium bromide (CTAB) was purchased from Sigma-Aldrich (USA). Strontium nitrate (Sr(NO<sub>3</sub>)<sub>2</sub>) was supplied from Tekkim (Turkey). All chemical reagents were used as received without further purification. Polypropylene (PP) - Ecolen HZ40P in pellet form was obtained from Hellenic Petroleum (Greece). It has a density and melt flow index of 0.90 g/cm<sup>3</sup> (ASTM D792) and 12 g/10 min (2.16 kg, 230 °C, ASTM D1238), respectively. Maleic anhydride-grafted polypropylene (MAPP) in pellet form was provided from Sigma-Aldrich (USA) with a maleic anhydride content of 8-10 wt.%, a density of 0.93 g/cm<sup>3</sup> and a melting point of 156 °C. Before using, PP and MAPP pellets were cut into granules with a size of about millimeter level using a chopper with milling blades to enhance the mixing efficiency during melt blending process. High-purity deionized water with a resistivity of 18.2 MΩ.cm (at 25 °C) was used in all procedures.

### 2.2. Synthesis of SHPs

Sr(NO<sub>3</sub>)<sub>2</sub> and (NH<sub>4</sub>)<sub>2</sub>HPO<sub>4</sub> were used as starting materials for hydrothermal synthesis of SHPs. Firstly, 63 g of Sr(NO<sub>3</sub>)<sub>2</sub> and 0.36 g of CTAB were dissolved in 400 ml deionized water under mechanical stirring for 20 min (solution A). Secondly, 33 g of (NH<sub>4</sub>)<sub>2</sub>HPO<sub>4</sub> was dissolved in 200 ml deionized water (solution B). Then A and B solutions were added to each other and stirred at room temperature (800 rpm for 20 min). The resulting suspension was kept in a pressure vessel at 90 °C for 6 h, and then left at room temperature for 12 h. The resulting white precipitate was filtered and washed with deionized water and ethanol several times. The obtained filter cake was dried in a static oven at 100 °C for 12 h, then ground, and sieved using a 45 μm sieve. β-SrHPO<sub>4</sub> platelets obtained were then stored in airtight plastic bags without applying any treatment, until they were dried for melt blending process. The above-mentioned process is the same as the protocol proposed by Zhuang et al. [24], but the quantities have been scaled up tenfold considering the amount of SHP required to produce the composites.

### 2.3. Production of PP/SHP Nanocomposites

Prior to the mixing step, PP, MAPP and SHPs were dried at 100 °C for 12 h to eliminate residual moisture. Four different SHPs content (1-3-5-7 wt.%) was used to produce PP/SHP nanocomposites. MAPP was added to the composites in the amount of 30% of the filler concentrations, as stated in Table 1. The copolymer/filler ratio is a suggested method to determine the amount of the required compatibilizer, and 30% ratio is taken from the literature [29]. The melt blending process was performed by using a laboratory type co-rotating twin screw extruder with a screw diameter of 12 mm, and a screw length (*L*) to diameter (*D*) ratio of 24 (Gulnar, Turkey). The barrel temperature profile of the extruder was set at 35-180-185-190-190-180 °C from the feeding zone to the die exit. The screw speed was fixed at 75 rpm. The rod-shaped composite product extruded from the die tip was hardened immediately by using a fan and chopped by an in-situ pelletizing unit. The obtained nanocomposite pellets were dried at a temperature of 100 °C for overnight to

remove the moisture content. The dried pellets then molded into the shape of test samples by an injection-molding machine (Xplore IM12, The Netherlands) with a barrel temperature of 200 °C. The mold temperature and injection pressure were 20 °C and 8 bars, respectively. For using as a control sample, pure PP was treated under the same conditions.

Table 1. The composition of the samples used in this study

Sample code	PP (wt.%)	MAPP (wt.%)	SHP (wt.%)
PP	100	0	0
PP/ 1SHP	98.7	0.3	1
PP/ 3SHP	96.1	0.9	3
PP/ 5SHP	93.5	1.5	5
PP/ 7SHP	90.9	2.1	7

#### 2.4. Structural Characterization

XRD patterns of SHPs were measured by using Bruker AXS-D8 Advanced (Germany) diffractometer using CuK $\alpha$  radiation ( $\lambda=1.5405$  Å) and 0.02° angle step. TGA measurements were carried out using Hitachi High-Tech STA7300 (Japan) under nitrogen atmosphere from ambient temperature up to 800 °C at a linear heating rate of 10 °C/min. PerkinElmer Spotlight 400 FTIR (USA) spectrometer was used to examine the functional groups vibrations of the SHPs at an optical resolution of 4 cm<sup>-1</sup>. Morphology of the samples was investigated using Zeiss Gemini 500 FE-SEM (Germany) at 3.0 kV after sputter coated with gold for conductivity.

#### 2.5. Mechanical Characterization

The tensile tests were performed using a tensile-compression test machine with 5 kN loading capacity (Devotrans GP/R/DNN/CKS-III, Turkey) according to ASTM D638. Tensile tests were carried out at 5 mm/min test speed using dog-bone shaped (type-V) samples. The flexural tests were carried out on the same machine according to ASTM D790 using a 2.54 mm/min cross-head speed. The dimension of the flexural samples was 125 mm in length, 12.7 mm in width and 3.2 mm in thickness, and a span of 55 mm was used in three-point bending mode. Shore D hardness measurements were also done according to ASTM D2240. At least four measurements were made for all tests and their averages and standard deviations were presented.

#### 2.6. Wear Tests

Wear tests were performed on the cylindrical samples of 8 mm in thickness and 30 mm in diameter using a custom build ball-on-disc wear tester at dry sliding friction (ASTM G99). Tribo-tests were conducted at ambient temperature of 25 ± 2 °C and the humidity of 25%. In tests, the ball was loaded horizontally to the ground against a vertically rotating composite disc to reduce the wear debris and third-body abrasive wear effect, as shown in Fig. 1. Similar studies on different materials that used similar test configurations can be found in the literature [30-32]. This type of configuration reduces the debris in the wear track and therefore contributes to keep the wear mechanism unchanged [33]. The samples were polished one side up to R<sub>a</sub>≈0.20 μm. ø5 mm Si<sub>3</sub>N<sub>4</sub> balls were used as counterparts due to its high hardness and no chemical affinity for the materials tested. Before each test, the surface of the samples and balls were cleaned by using alcohol and dried carefully. The normal load was selected as 5 N, and the disc speed was selected as 1100 rpm which corresponds to 0.7 m/s sliding speed in the center of the wear track. Wear tests were ended

at 420 m sliding distance which corresponds to a 10 min test duration. The volume loss  $V$  ( $\text{mm}^3$ ) and the wear rate  $K$  ( $\text{mm}^3 \text{N}^{-1} \text{m}^{-1}$ ) of the samples were obtained from the Eq. 1 and Eq. 2, respectively [34]. Here,  $b$  and  $d$  are the track width and diameter (mm), respectively,  $r$  is the radius of the  $\text{Si}_3\text{N}_4$  ball (mm),  $F$  is the vertical load (N), and  $S$  is the ball sliding distance (m). Wear track diameter was fixed at 12 mm in all the tests. The average wear track widths were calculated using the “trapezoidal area model” described elsewhere [35]. The steady-state coefficient of friction (CoF) values of the samples were also obtained from a load cell sensor and compared according to SHP concentration. After the test, worn surfaces of the samples were investigated with optical microscopy and their wear mechanisms were compared.

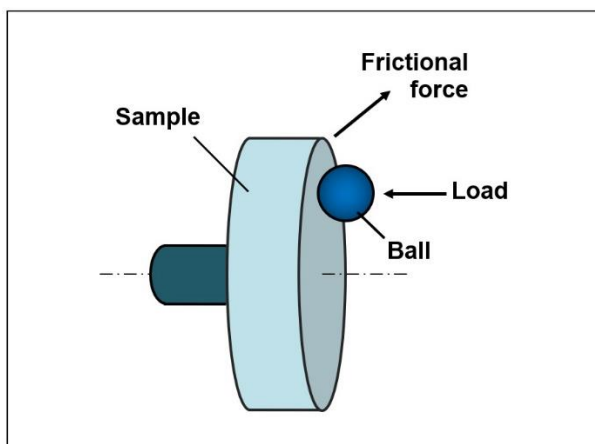


Fig. 1 Ball-on-disc test configuration

$$V = \left[ \frac{\pi r^2}{180} \arcsin\left(\frac{b}{2r}\right) - \frac{b}{2} \sqrt{r^2 - \frac{b^2}{4}} \right] \pi d \quad (1)$$

$$K = \frac{V}{FS} \quad (2)$$

### 3. Results and Discussion

#### 3.1. SHP Morphology and Structure

The XRD results revealed that SHPs successfully synthesized at high purity as seen in Fig. 2a. All the diffraction peaks of SHP were indexed according to the reported crystal structure of  $\beta$ - $\text{SrHPO}_4$  (JCPDS 12-0368) with hexagonal crystal structure and no foreign peak was detected. This result is in good agreement with the observations reported by Zhuang et al. [24]. The morphology of SHPs observed by SEM is composed of regular nanosheets as seen in Fig. 2b. The thickness of SHPs was in the range of 35-50 nm. FTIR spectra was used to confirm the presence of characteristic absorption bands of SHPs. The weak bands at  $2998 \text{ cm}^{-1}$  and  $1785 \text{ cm}^{-1}$  in Fig. 2c arise from the vibration of hydrogen bridge bonds. The peaks between  $1300 \text{ cm}^{-1}$  and  $500 \text{ cm}^{-1}$  are ascribed to  $\nu(\text{PO}_4)$ ,  $\delta(\text{PO}_4)$  and  $\delta(\text{O-H})$  vibrations [25]. TGA is a tool to assess the thermal stability of a material by monitoring the mass loss during heating of a sample at controlled heating rate. The TGA and corresponding DTG curves of SHPs are shown in Fig. 2d. It is obvious that SHP

degrades mainly in two steps with maximum rates at 376 °C and 587 °C, according to following reactions [23]:



In the first degradation step, SHPs decompose into hydrated strontium pyrophosphate and water (Eq. 3). In the second step, dehydrated strontium pyrophosphate continues to decompose into  $\beta$ -strontium pyrophosphate and water (Eq. 4). According to the results, total weight loss till 800 °C is only 5.2% which indicates that SHP has a high thermal stability.

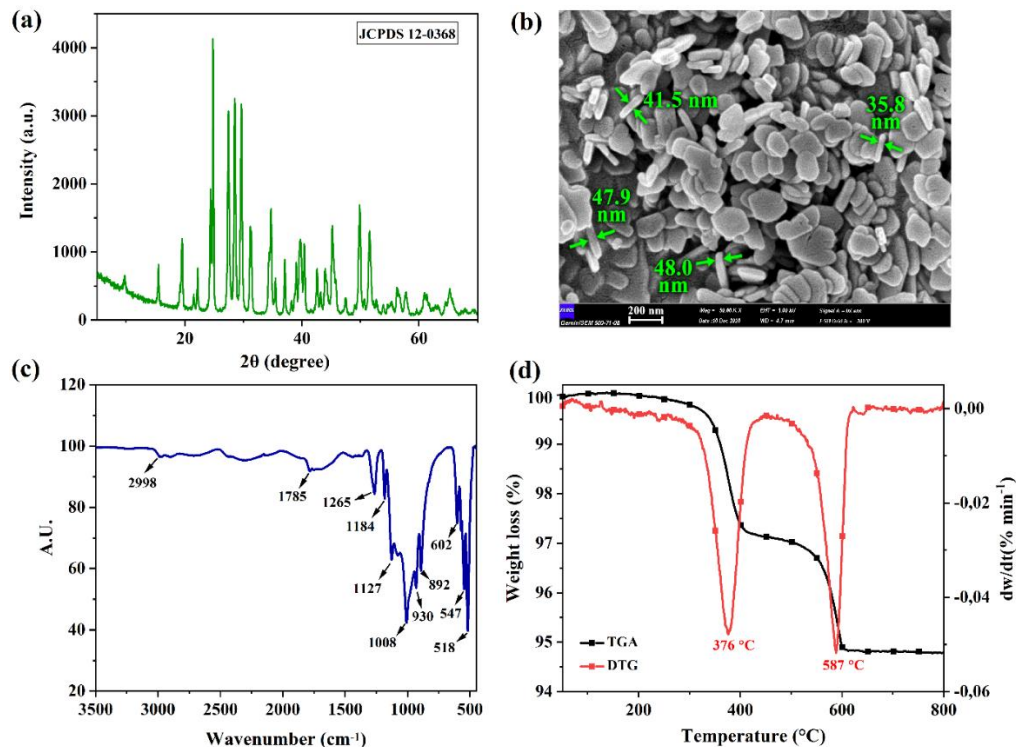


Fig. 2 (a) XRD pattern, (b) SEM image, (c) FTIR spectra, (d) TGA and DTG graphs of SHPs

### 3.2. Thermal Properties of PP/SHP Nanocomposites

One of the important features for the detection of the multifunctionality of polymer composites is thermal stability. TGA and dTGA curves of pure PP and PP/SHP nanocomposites are shown in Fig. 3a and Fig. 3b, respectively, and related data about residues and temperatures corresponding to 5% ( $T_{5\%}$ ) and maximum degradation rates ( $T_{max}$ ), which are used to evaluate the decomposition of the samples are summarized in Table 2. The pure PP only exhibits one step stage (at 457 °C) which is attributed to the decomposition of macromolecule chains [36]. The addition of SHPs was also found to have no effect on the thermal degradation profiles of the composites, and they showed one step mass loss stage with maximum rates at between 458 °C and 464 °C. However, the incorporation of SHPs leads to a slight shift toward higher  $T_{5\%}$  and  $T_{max}$  values in comparison with that of pure PP. This behavior indicates that the addition of SHPs leads to

an improvement in thermal stability of PP/SHP nanocomposites. This is attributed to the barrier effect of the sheet structure of SHPs which reduces the heat conduction in the PP and inhibits the diffusion of the volatile degradation products from the polymer onto the gas phase [12, 13]. The char yield of PP/SHP nanocomposites was increased with identical filler content. As summarized in Table 2, PP showed a char residue of 3.07% at 800 °C, but PP/SHP nanocomposites showed an improvement in the char yield in the range of 43.9-73.8% compared to that of pure PP, possibly due to the catalytic carbonization effect of SHPs.

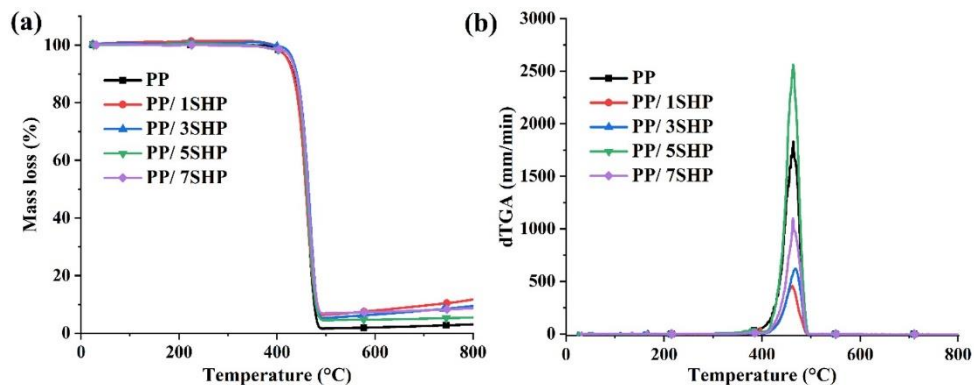


Fig. 3 (a) TGA and (b) dTGA curves of PP and PP/SHP nanocomposites

Table 2. TGA results of the samples

Sample code	$T_{5\%}$ (°C)	$T_{max}$ (°C)	Char yield (%)
PP	418	457	3.07
PP/ 1SHP	421	458	11.73
PP/ 3SHP	429	464	9.57
PP/ 5SHP	428	460	5.48
PP/ 7SHP	428	463	8.72

### 3.3. Tensile and Flexural Properties of PP/SHP Nanocomposites

The morphological analysis of the fracture surface of PP/SHP nanocomposites with different SHP content is presented in Fig. 4. When SEM micrographs are examined, it is understood that there are different regions where SHPs are uniformly distributed and also coagulated in PP matrix. It was determined that the number of coagulated particles increased with the increase in SHP concentration in the composites. While the coagulated particles are few as seen in Fig. 4a-I, there can be tens of them as indicated by the purple arrows in Fig. 4b with the increase in SHP concentration. Despite the compatibilizer used, SHPs were tended to self-aggregate with the increase in concentration and form nano/micron sized particulates. This is a situation that may adversely affect the mechanical properties of PP/SHP nanocomposites. However, it is noteworthy that there is also a linear increase in the number of homogeneously distributed individual particles. Looking closely at micrographs, it is possible to see homogeneously dispersed particles in PP matrix for all concentrations as seen in Fig. 4b-II and as indicated by yellow arrows in Fig. 4d. Similar phenomena have been previously reported in studies using non-polar polymers [13]. Although various factors may be effective in the low mixing efficiency in polymer nanocomposites, the insufficient shear stresses in laboratory type twin screw extruders and screw configuration is considered one of the main reasons. Despite the partially poor dispersion of SHPs observed in all composites, it is understood that the use

of compatibilizer increases the adhesion efficiency of even coagulated particles with PP matrix by forming polymer branches adhering to particulates as seen in the detailed view in Fig. 4d-III.

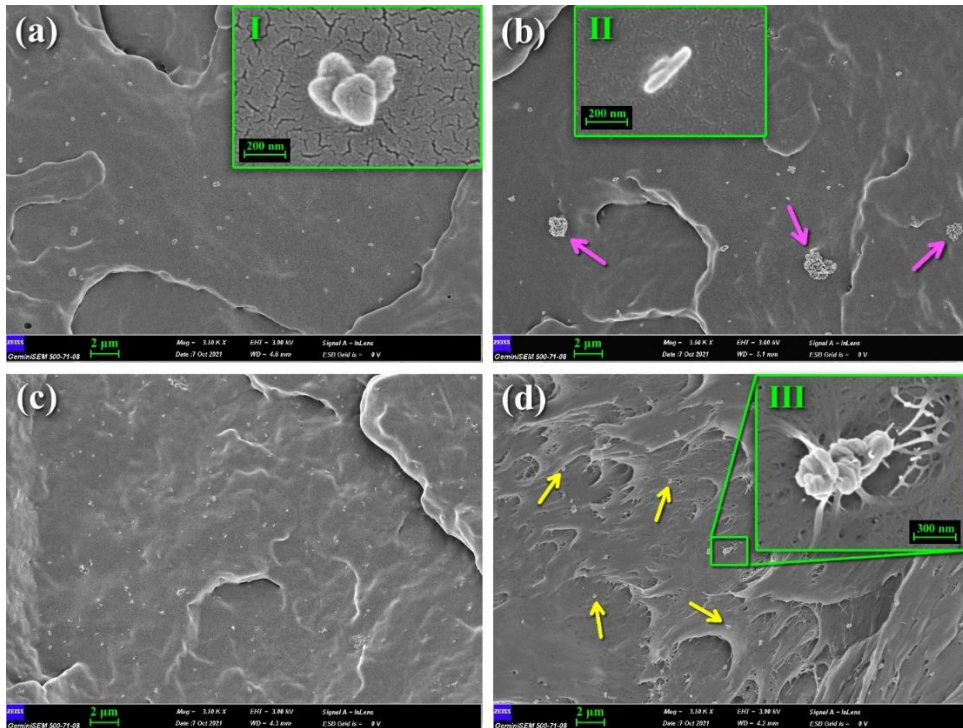


Fig. 4 SEM micrographs of the fracture surfaces of the nanocomposites: (a) PP/ 1SHP, (b) PP/ 3SHP, (c) PP/ 5SHP, and (d) PP/ 7SHP

Hardness is known as an important indicator of mechanical and wear behaviors of polymer composites. Shore D hardness values of pure PP and PP/SHP nanocomposites is given in Fig. 5. It was found that the hardness values of the nanocomposites were higher than that of pure PP for each filler content. It is already known that the addition of hard particles into a relatively soft structure will result in an increase in hardness and stiffness [37]. Although a linear increase was observed at low concentrations, no significant change was found after 3 wt.% SHP concentration. At 7 wt.% SHP content, the hardness of 73.1 Shore D was achieved. Considering the indentation depth and contact area of the Shore D tip used in the hardness measurement, it is understood that the particles are distributed homogeneously enough to affect the general rigidity of the structure, even if there is some agglomeration in the composite structure.

The tensile and flexural test graphs of the samples are given in Fig. 6, and related test data are summarized in Table 3. PP exhibited a tensile strength of 44.8 MPa, and a tensile modulus of 582.2 MPa. The incorporation of SHP into the structure caused an increase in tensile strength of the composites. The highest tensile strength value of 47.5 MPa was observed at 7 wt.% SHP content. At this concentration, the increase in tensile strength compared to the pristine polymer is about 6.0%. It is well known that relatively rigid structure of nanoparticles in a soft polymer matrix causes effects such as absorption of energy and prevention of crack formation, which has positive results on mechanical properties of the composites if the particle distribution is homogeneous and the adhesion

among the constituents is strong enough [21]. Moreover, large surface-active centers of SHPs cause more physical and chemical interactions with the matrix material [38].

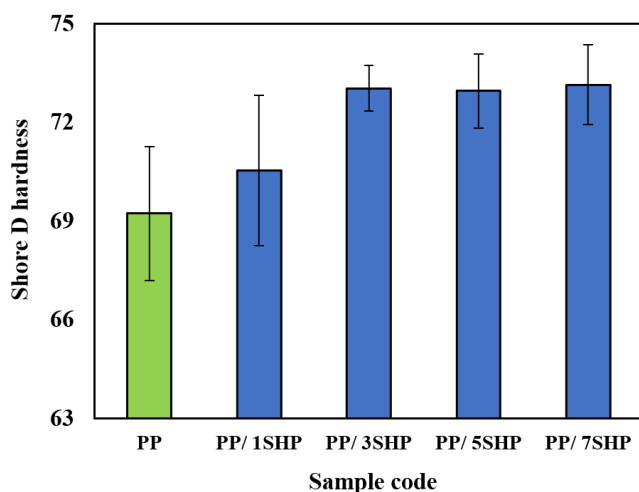


Fig. 5 Shore D hardness values of PP and PP/SHP nanocomposites

The increment in elastic modulus appeared in different magnitudes at various SHP concentration. It is thought that the reduction in exfoliation level and increase in rigid filler content compensate each other. The highest elastic modulus of 698.5 MPa was found at the composite with 1 wt.% SHP concentration. It is well known that the increment in elastic modulus is attributed to the high aspect ratio of nanofillers used in polymer nanocomposites. This behavior has been described in a similar study and explained by the two-dimensional geometry of nanosheets. Achaby and Qaiss [12] observed the same effect for graphene nanosheets in polyethylene matrix. Although there is no linear change according to the amount of reinforcement, it was determined that the elongation at break values decreased with the increase in stiffness in the composites compared to pure PP. Although the tensile strength increased, this caused the transition from ductile to brittle fracture. Conversely, ductile PP showed very high elongation value with the alignment of polymer chains along the longitudinal axis of the tensile test sample. The elongation at break of PP reduced from 615% to about 22% at 7 wt.% SHP concentration. Although no meaningful change was observed depending on the filler concentration, SHPs were seen to act as physical crosslinking points in polymer matrix and restrict the movement of PP chains, leading PP/SHP nanocomposites deformed in a brittle manner. A similar behavior was reported by Roserh et al. [39] where the percentage of elongation at break decreases with increasing graphite nanosheets content in PP matrix.

Table 3. Mechanical properties of the samples

Sample code	Tensile properties			Flexural properties		
	Tensile strength (MPa)	Tensile modulus (MPa)	Elongation at break (%)	Flexural strength (MPa)	Flexural modulus (MPa)	Elongation at break (%)
PP	44.8 ± 0.9	582.2 ± 26.4	614.9 ± 91.9	46.3 ± 1.4	1330.5 ± 105.0	-
PP/ 1SHP	46.4 ± 1.1	698.5 ± 43.6	20.5 ± 6.7	46.2 ± 1.0	1386.8 ± 58.8	-
PP/ 3SHP	45.8 ± 0.3	641.7 ± 41.6	23.0 ± 1.3	47.5 ± 0.4	1465.0 ± 113.4	-
PP/ 5SHP	45.5 ± 1.1	615.8 ± 112.2	20.0 ± 1.6	49.1 ± 1.2	1465.5 ± 142.1	-
PP/ 7SHP	47.5 ± 1.7	686.6 ± 123.4	22.4 ± 2.6	46.8 ± 2.7	1477.2 ± 76.2	-

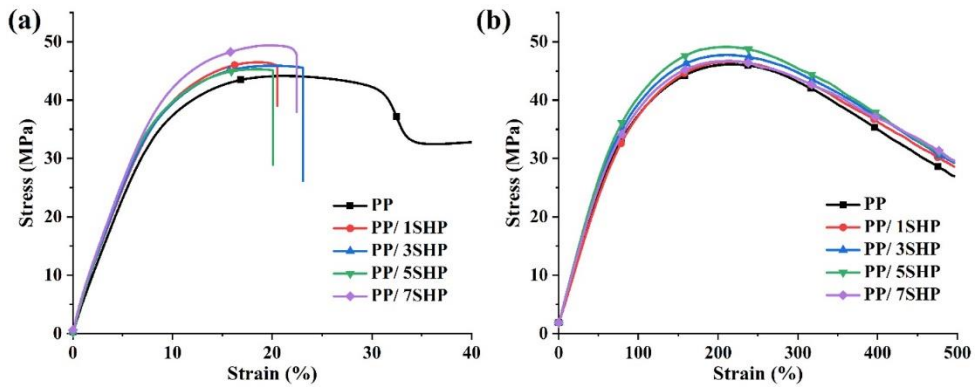


Fig. 6 (a) Tensile and (b) flexural stress-strain curves of PP and PP/SHP nanocomposites

Apart from the tensile test, flexural tests also give a good outlook on the mechanical properties of materials under the combination of tensile and compression loads. As seen in Fig. 6b, all samples reach a maximum loading capacity up to a certain strain value, and then the stress gradually decreases. The flexural strength and modulus values of PP are 46.3 MPa and 1330.5 MPa, respectively. No significant change was observed in the flexural strength of the composite with the addition of 1 wt.% SHP. After this concentration, flexural strength of the composites increased to a maximum value of 49.1 MPa for 5 wt.% SHP concentration. It is noteworthy that the flexural strength decreased again after this concentration. Although nano- and micro-agglomerations were evident from the SEM micrographs of the composites, SHPs were thought to show reinforcing effect and enhance the flexural strength of PP with the contribution of individual particulates homogeneously dispersed in the structure. In polymer composites, stress is transmitted from the matrix to the filler via interface; hence, good adhesion between the fillers and matrix allows for more efficient transfer of energy and leads to enhanced mechanical properties. The increase in flexural strength indicates that the efficient load transfer from the matrix to individual SHP particulates is occurred under the stress applied in the test. However, relatively dense characteristic of SHP due to the presence of metallic atoms in the structure adversely influences the final mechanical properties of the composites, thus an inhomogeneous stress distribution occurs within PP. This behavior was described by Zahibi and co-workers for 2D bauxite nanosheets in an epoxy matrix [5]. Flexural modulus of the composites were found to increase with filler concentration, and the highest modulus of about 1477 MPa was achieved at 7 wt.% SHP content. The composite elastic modulus is mainly dependent on the volumetric fraction of the filler in the composite, together with the intrinsic stiffness of the matrix and filler. The increment in the modulus is expected due to the high stiffness of the SHPs compared to pure PP. At the end of the flexural tests, none of the samples were broken within a 25 mm strain limit. During flexural test where the material is exposed to compression and shear forces in addition to tensile forces, the cracks do not exert such a key role as in the case of tensile test. As said before, decrease in the elongation at break values of PP/SHP nanocomposites arise from the fact that SHPs restrict the mobility of PP chains. In the light of these findings, the improvement both in the tensile and flexural strength of the composites can mainly attributed to the rigid 2D sheet nature of the filler. These observations are consistent with the conclusions found in previous studies [5, 10, 12, 17, 38]. It is also thought that the level of homogeneous distribution of individual particulates in the composite structure is responsible for the improvements observed at different SHP concentrations. However, along with the results obtained, there are other factors to be considered such as production method, surface treatment and concentration of the nanosheets. Although these issues still need to be explored, in

summary, tensile and flexural test results seem to be promising about the reinforcing potentiality of SHPs.

### 3.4. Wear Properties of PP/SHP Nanocomposites

CoF versus sliding time curves of the nanocomposites are shown in Fig. 7a. Average CoF values and wear rates of the samples with different SHPs concentrations are given in Fig. 7b and Fig. 7c, respectively. Fig. 7a indicates that all the CoFs reach nearly a steady state condition after about 200 s sliding time, which is corresponding to 140 m sliding distance. The characteristic structures of the CoF curves of the samples throughout the sliding distance were generally similar to each other, and no distinctive difference was observed. However, a slight fluctuation in the CoF curve of the sample containing 5 wt.% SHP is noticeable, and the highest CoF of 0.47 was reached at this concentration.

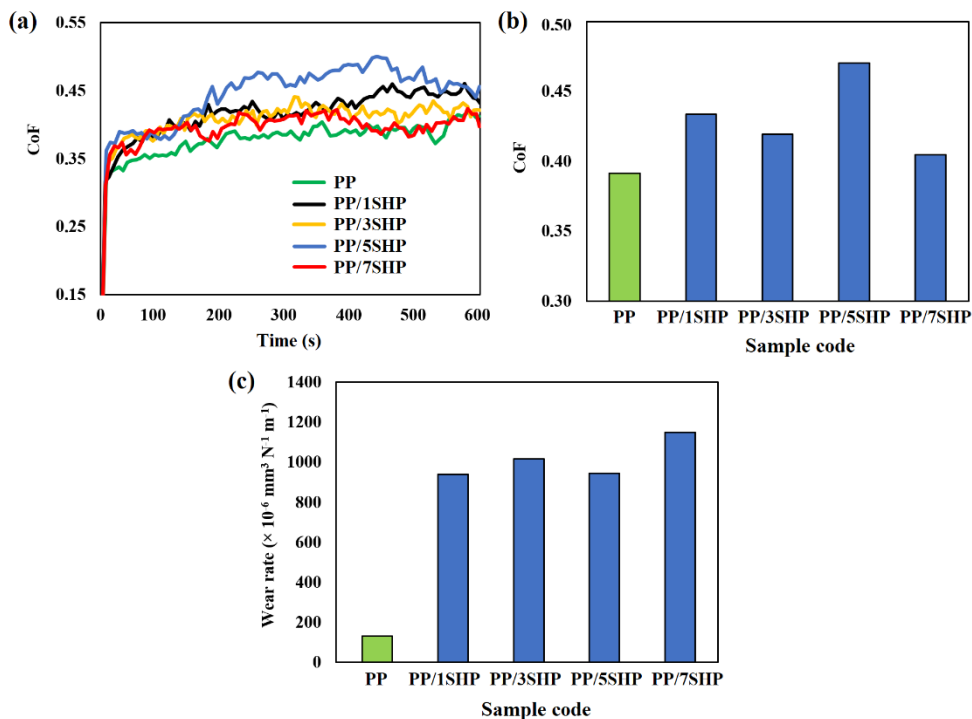


Fig. 7 (a) CoF versus sliding time curves, (b) average CoF, and (c) wear rate values of PP and PP/SHP nanocomposites

It is clearly seen in Fig. 7b and c that CoFs and wear rates of the nanocomposites are both higher than those of the pure PP. PP/ 7SHP showed the lowest CoF value of 0.40, but highest wear rate of  $K = 1151 \times 10^{-6} \text{ mm}^3 \text{ N}^{-1} \text{ m}^{-1}$  among the composites tested. However, no meaningful change was observed in CoF and wear rates depending on the SHP concentration. There is generally a close relationship between mechanical properties and sliding wear resistance of polymer composites. If the strength and modulus of polymers are increased with reinforcements, improvement in wear resistance should also be expected [40]. However, the literature regarding the wear mechanisms of nanoplatelet reinforced composites has been quite scarce. While the wear resistance of particulate reinforced polymer composites improves with good interfacial bonding between filler and matrix, it can vary with the volume fraction of fillers depending on the filler and matrix type.

In addition, polymers have different wear characteristics from metals and ceramics due to their viscoelastic nature and their ability to transfer material easily to the counterparts [41]. In polymer composites, fillers are also included in this phenomenon and may show abrasive effect depending on sliding conditions as stated before. This explains why the wear rates of the composites are higher compared to that of pure PP.

Worn surfaces of the samples are shown in Fig. 8. Some color adjustments were made on the images to expose the wear tracks clearly. It is seen that the worn area in contact with the ball is much rougher than the unworn sample surface, due to micro-plowing and micro-cutting actions formed by abrasion. It was also found that micro and macro size scratches were observed in the sliding direction of the ball in all samples because of the same abrasive wear mechanism. In addition, the stuck wear debris was found on the wear tracks of the samples despite the vertical configuration of the test rig. Although the wear tracks of the samples had similar longitudinal scratches, signs of plastic deformation and adhesive wear were also observed. However, when the SHP concentration is taken into consideration, it is seen that there are certain changes in the wear characteristics of the nanocomposites. It is obvious from Fig. 8d and Fig. 8e that adhesive wear and plastic deformation observed especially at the edges of the wear tracks at higher SHP concentrations (5 and 7 wt.%). In polymer composites, beside adhesive and abrasive wear mechanisms, the fatigue wave or crack formation is another wear phenomenon. Such findings are often seen due to fatigue wear caused by repeated cycles of an asperity of the counter material on the worn surface. Fatigue wear also increases with increasing stress or defect concentration on the sample [42].

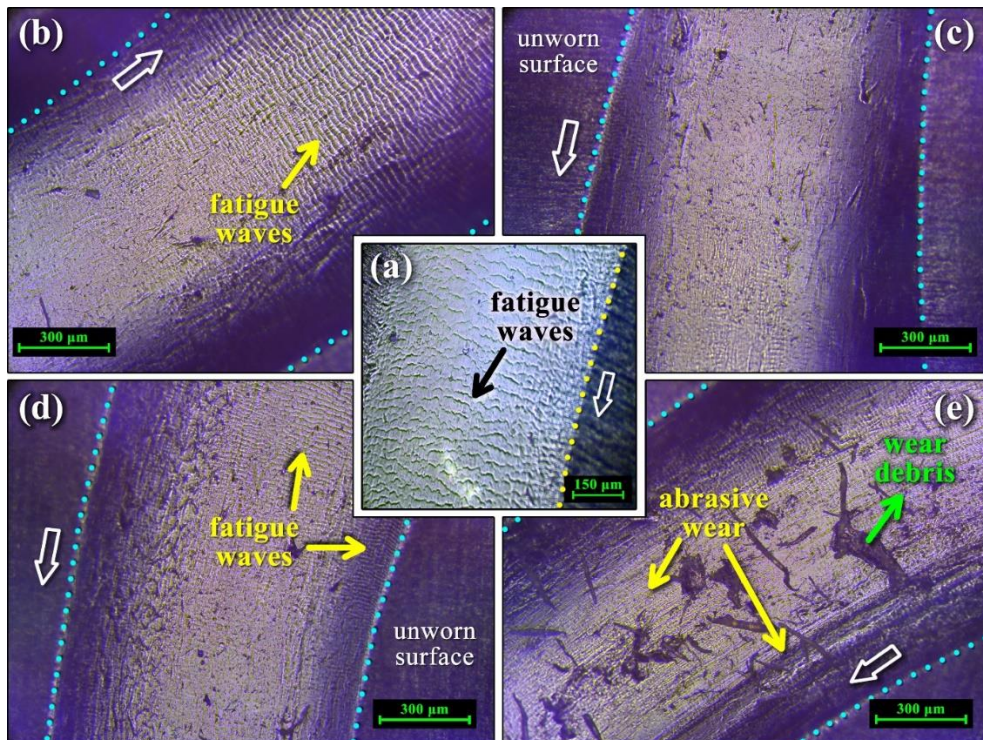


Fig. 8 Optic microscope images of the worn surface of pure PP and the nanocomposite samples: (a) PP, (b) PP/ 1SHP, (c) PP/ 3SHP, (d) PP/ 5SHP, and (e) PP/ 7SHP (the blank arrows indicate the sliding direction of the ball)

Looking closely at Fig. 8a, Fig. 8b and Fig. 8c, while many fatigue waves are observed in PP, PP/ 1SHP and PP/ 3SHP samples, it is seen that they decrease in higher SHP concentrations. In addition, segments where the transition from fatigue wear to abrasive wear occurred in different parts of the wear track were determined in all samples. On the other hand, it has been found that abrasive wear and micro-scratches are dominant due to the relatively higher rigidity of the nanocomposites at higher filler concentrations originating from SHP. As stated before, it is clear that rigid SHP as the third-body element in the wear system increases the wear rate due to the abrasive wear effect with micro-cutting and micro-plowing actions.

#### 4. Conclusions

After SHPs were synthesized by hydrothermal method, PP/SHP composites were successfully produced via melt blending technique for the first time. The effects of filler concentration on the thermal, mechanical and tribological properties of the composites have led to the following conclusions:

- SHPs are conducive to improving the thermal stability of PP/SHP composites. With the loading of 3 wt.% SHPs,  $T_{5\%}$  and  $T_{max}$  values of the composites were increased by 11 °C and 7 °C, respectively, compared to pure PP. In addition, introduction of SHPs clearly enhanced the residue formation of PP/SHP composites.
- SHPs in PP also showed a noticeable difference in mechanical properties of the samples, even if coagulated particulates are seen in the structure. The highest tensile and flexural strengths of 47.5 and 49.1 MPa was achieved at the composites with 7 and 5 wt.% SHP concentration, respectively.
- In addition, an increase was observed in elastic modulus of the composites compared to pure PP. The improvement in mechanical properties is thought to be due to the rigid 2D structure of SHPs which leads to more contact area with polymer chains and leads to higher resistance especially against compression load, even at high agglomeration rates.
- From the wear test results, the transition from fatigue wear to abrasive wear was observed after 3 wt.% SHP concentration due to the increase in composite hardness. The high rigidity of SHP compared to the pure polymer increased the micro-plowing phenomenon in contact with the counter material. Therefore, an increase was observed in the CoF and wear rates of the composites, independent of the SHP concentration. However, it is thought that the high resistance to fatigue wear obtained at high SHP concentrations may be advantageous for different applications.

#### Acknowledgement

This work is supported by Erciyes University Scientific Research Unit under grant no BAP-FKB-2020-9952.

#### References

- [1] Bhattachary M. Polymer nanocomposites-A comparison between carbon nanotubes, graphene, and clay as nanofillers. *Materials*, 2016; 9(4): 262. <https://doi.org/10.3390/ma9040262>
- [2] Brevnov PN, Kirsankina GR, Zabolotnov AS, Krashennikov VG, Grinev VG, Berezkina NG, Sinevich EA, Shcherbina MA, Novokshonova LA. Synthesis and properties of nanocomposite materials based on ultra-high-molecular-weight polyethylene and

- graphite nanoplates. *Polymer Science, Series C*, 2016; 58: 38-49. <https://doi.org/10.1134/S1811238216010021>
- [3] Mochane MJ, Magagula SI, Sefadi JS, Sadiku ER, Mokhena TC. Morphology, Thermal Stability, and Flammability Properties of Polymer-Layered Double Hydroxide (LDH) Nanocomposites: A Review. *Crystals*, 2020; 10(7): 612. <https://doi.org/10.3390/cryst10070612>
- [4] Rathod V, Kumar JS, Jain A. Polymer and ceramic nanocomposites for aerospace applications. *Applied Nanoscience*, 2017; 7: 519-548. <https://doi.org/10.1007/s13204-017-0592-9>
- [5] Zabihi O, Ahmadi M, Ferdowsi MRG, Li Q, Fakhrhoseini SM, Mahmoodi R, Ellis AV Naebe M. Natural bauxite nanosheets: A multifunctional and sustainable 2D nano-reinforcement for high performance polymer nanocomposites. *Composites Science and Technology* 2019; 184: 107868. <https://doi.org/10.1016/j.compscitech.2019.107868>
- [6] Saxena N. Thermal and mechanical behavior of polymer nano-composite. *Journal of Polymer Engineering*, 2010; 30: 575-586. <https://doi.org/10.1515/POLYENG.2010.30.9.575>
- [7] Gharabaghi H, Rafizadeh M, Taromi FA. Synthesis of exfoliated PA66 nanocomposites via interfacial polycondensation: effect of layered silicate and silica nanoparticles. *Bulletin of Materials Science*, 2016; 39: 935-941. <https://doi.org/10.1007/s12034-016-1228-5>
- [8] Yetkin SH. Tribological properties of compatibilizer and graphene oxide-filled polypropylene nanocomposites. *Bulletin of Materials Science*, 2020; 43: 89. <https://doi.org/10.1007/s12034-020-2061-4>
- [9] Jordan J, Jacob KI, Tannenbaum R, Sharaf MA, Jasiuk I. Experimental trends in polymer nanocomposites-a review. *Materials Science and Engineering A*, 2005; 393: 1-11. <https://doi.org/10.1016/j.msea.2004.09.044>
- [10] Varghese AM, Singh S, Rangaraj VM Mittal V. Two-dimensional mullite nanostructure: Synthesis and reinforcement effect on polypropylene/maleic anhydride graft ethylene vinyl acetate matrix. *Journal of Applied Polymer Science*, 2019; 136: 48233. <https://doi.org/10.1002/app.48233>
- [11] Xu Z, Shen X, Wang T, Yang Y, Yi J, Cao M, Shen J, Xiao Y, Guan J, Jiang X, Tang B, Li H. Investigation on tribological and thermo-mechanical properties of Ti3C2 nanosheets/epoxy nanocomposites *ACS Omega*, 2021; 43: 29184-29191. <https://doi.org/10.1021/acsomega.1c04620>
- [12] Achaby ME, Qasis A. Processing and properties of polyethylene reinforced by graphene nanosheets and carbon nanotubes. *Materials and Design*, 2013; 44: 81-89. <https://doi.org/10.1016/j.matdes.2012.07.065>
- [13] Li CQ, Zha JW, Long HQ, Wang SJ, Zhang DL, Dang ZM. Mechanical and dielectric properties of graphene incorporated polypropylene nanocomposites using polypropylene-graft-maleic anhydride as a compatibilizer. *Composites Science and Technology*, 2017; 153: 111-118. <https://doi.org/10.1016/j.compscitech.2017.10.015>
- [14] Burmistr MV, Sukhyy KM, Shilov VV, Pissis P, Spanoudaki A, Sukha IV, Tomilo VI, Gomza YP. Synthesis, structure, thermal and mechanical properties of nanocomposites based on linear polymers and layered silicates modified by polymeric quaternary ammonium salts (ionenes). *Polymer*, 2005; 46: 12226-12232. <https://doi.org/10.1016/j.polymer.2005.10.094>
- [15] Lonkar SP, Therias S, Leroux F, Gardette JL, Singh RP. Thermal, mechanical, and rheological characterization of polypropylene/layered double hydroxide nanocomposites. *Polymer Engineering and Science*, 2012; 52: 2006-2014. <https://doi.org/10.1002/pen.23147>
- [16] Chen L, Chen B, Li J, Tong X, Zhao H, Wang L. Enhancement of mechanical and wear resistance performance in hexagonal boron nitride-reinforced epoxy nanocomposites. *Polymer International*, 2017; 66: 659-664. <https://doi.org/10.1002/pi.5296>

- [17] Feng X, Xing W, Liu J, Qiu S, Hu Y, Liew KM. Reinforcement of organo-modified molybdenum disulfide nanosheets on the mechanical and thermal properties of polyurethane acrylate films. *Composites Science and Technology*, 2016; 137: 188-195. <https://doi.org/10.1016/j.compscitech.2016.11.002>
- [18] Wadi VS, Jena KK, Haliq K, Alhassan SM. Enhanced mechanical toughness of isotactic polypropylene using bulk molybdenum disulfide. *ACS Omega*, 2020; 5: 11394-11401. <https://doi.org/10.1021/acsomega.0c00419>
- [19] Sun H, Fang Z, Li T, Lei F, Jiang F, Li D, Zhou Y, Sun D. Enhanced mechanical and tribological performance of PA66 nanocomposites containing 2D layered  $\alpha$ -zirconium phosphate nanoplatelets with different sizes. *Advanced Composites and Hybrid Materials*, 2019; 2: 407-422. <https://doi.org/10.1007/s42114-019-00100-z>
- [20] Zhang R, Hu Y, Li B, Chen Z, Fan W. Studies on the preparation and structure of polyacrylamide/ $\alpha$ -zirconium phosphate nanocomposites. *Journal of Materials Science*, 2007; 42: 5641-5646. <https://doi.org/10.1007/s10853-006-0629-z>
- [21] Zhang H, Wang L, Chen Q, Li P, Zhou A, Cao X, Hu Q. Preparation, mechanical and anti-friction performance of MXene/polymer composites. *Materials and Design*, 2016; 92: 682-689. <https://doi.org/10.1016/j.matdes.2015.12.084>
- [22] Feng X, Wang B, Wang X, Wen P, Cai W, Hu Y, Liew KM. Molybdenum disulfide nanosheets as barrier enhancing nanofillers in thermal decomposition of polypropylene composites. *Chemical Engineering Journal*, 2016; 295: 278-287. <https://doi.org/10.1016/j.cej.2016.03.059>
- [23] Ropp RC, Aia A, Hoffman CWW, Veleker TJ, Mooney RW. X-Ray powder diffraction patterns of strontium phosphates. *Analytical Chemistry*, 1959; 31: 1163-1166. <https://doi.org/10.1021/ac60151a026>
- [24] Zhuang FQ, Tan RQ, Shen WF, Zhang XP, Xu W, Song WJ. Synthesis of  $\beta$ -type strontium hydrogen phosphate nanosheets and its immobilization of  $Pb^{2+}$  in acidic aqueous solution. *Acta Metallurgica Sinica*, 2015; 28(4): 438-443. <https://doi.org/10.1007/s40195-015-0214-z>
- [25] Roming M, Feldmann C. Selective synthesis of  $\alpha$ - and  $\beta$ -SrHPO<sub>4</sub> nanoparticles. *Journal of Materials Science*, 2008; 43: 5504-5507. <https://doi.org/10.1007/s10853-008-2830-8>
- [26] Boanini E, Gazzano M, Rubini K, Mazzeo PP, Bigi A. Structural interplay between strontium and calcium in  $\alpha$ -CaHPO<sub>4</sub> and  $\beta$ -SrHPO<sub>4</sub>. *Ceramics International*, 2021; 47: 24412-24420. <https://doi.org/10.1016/j.ceramint.2021.05.156>
- [27] Shi Y, Liu C, Liu L, Fu L, Yu B, Lv Y, Yang F, Song P. Strengthening, toughening and thermally stable ultra-thin MXene nanosheets/ polypropylene nanocomposites via nanoconfinement. *Chemical Engineering Journal*, 2019; 378: 122267. <https://doi.org/10.1016/j.cej.2019.122267>
- [28] Shubhra QTH, Alam AKMN, Quaiyyum MA. Mechanical properties of polypropylene composites: A review. *Journal of Thermoplastic Composite Materials*, 2011; 26: 362-391. <https://doi.org/10.1177/0892705711428659>
- [29] El-Sabbagh A. Effect of coupling agent on natural fibre in natural fibre/polypropylene composites on mechanical and thermal behaviour. *Compos Part B - Engineering*, 2014; 57: 126-135. <https://doi.org/10.1016/j.compositesb.2013.09.047>
- [30] Liu T, Wood W, Li B, Lively B, Zhong W-H. Effect of reinforcement on wear debris of carbon nanofiber/high density polyethylene composites: Morphological study and quantitative analysis. *Wear*, 2012; 294-295: 326-335. <https://doi.org/10.1016/j.wear.2012.07.010>
- [31] Prasad BK. Sliding wear behaviour of bronzes under varying material composition, microstructure and test conditions. *Wear*, 2004; 257: 110-123. <https://doi.org/10.1016/j.wear.2003.10.021>

- [32] Zhang LC, Zarudi I, Xiao KQ. Novel behaviour of friction and wear of epoxy composites reinforced by carbon nanotubes. *Wear*, 2006; 261: 806-811. <https://doi.org/10.1016/j.wear.2006.01.033>
- [33] Devaraju A, Perumal AE, Alphonsa J, Kailas SV, Venugopal S. Sliding wear behavior of plasma nitrided austenitic stainless steel type AISI 316LN in the temperature range from 25 to 400 °C at 10<sup>-4</sup> bar. *Wear*, 2012; 288: 17-26. <https://doi.org/10.1016/j.wear.2012.03.002>
- [34] Taktak S, Akbulut H. Dry wear and friction behaviour of plasma nitrided Ti-6AL-4 V alloy after explosive shock treatment. *Tribology International*, 2007; 40: 423-432. <https://doi.org/10.1016/j.triboint.2006.02.060>
- [35]avaş S, Al-Obaidi A. Influence of PP-g-MA compatibilization on the mechanical and wear properties of polypropylene/thermoplastic polyurethane blends. *Tribology Transaction*, 2018; 61: 754-764. <https://doi.org/10.1080/10402004.2017.1406173>
- [36] Yuan B, Hu Y, Chen X, Shi Y, Niu Y, Zhang Y, He S, Dai H. Dual modification of graphene by polymeric flame retardant and Ni (OH)<sub>2</sub> nanosheets for improving flame retardancy of polypropylene. *Composites Part A*, 2017; 100: 106-117. <https://doi.org/10.1016/j.compositesa.2017.04.012>
- [37] Fu SY, Feng XQ, Lauke B, Mai YW. Effects of particle size, particle/matrix interface adhesion and particle loading on mechanical properties of particulate-polymer composites. *Composites Part B: Engineering*, 2008; 39: 933-961. <https://doi.org/10.1016/j.compositesb.2008.01.002>
- [38] Wang Y, Gao J, Ma Y, Agarwal US. Study on mechanical properties, thermal stability and crystallization behavior of PET/MMT nanocomposites. *Composites Part B*, 2006; 37: 399-407. <https://doi.org/10.1016/j.compositesb.2006.02.014>
- [39] Roserh D, Gribbe GA, Luinstra GA. Graphite nanosheets-polypropylene composites from in toluene delaminated graphite using atactic polypropylene as dispersant. *Composites Science Technology*, 2018; 156: 28-38. <https://doi.org/10.1016/j.compscitech.2017.12.023>
- [40] Morioka Y, Tsuchiya Y, Shioya M. Correlations between the abrasive wear, fatigue, and tensile properties of filler-dispersed polyamide 6. *Wear*, 2015; 338: 297-306. <https://doi.org/10.1016/j.wear.2015.07.003>
- [41] Österle W, Dmitrev AI, Wetzel B, Zhang G, Häusler I, Jim BC. The role of carbon fibers and silica nanoparticles on friction and wear reduction of an advanced polymer matrix composite. *Materials Design*, 2016; 93: 474-484. <https://doi.org/10.1016/j.matdes.2015.12.175>
- [42] Myshkin NK, Petrokovets MI and Kovalev AV. Tribology of polymers: Adhesion, friction, wear, and mass-transfer. *Tribology International*, 2005; 38: 910-921. <https://doi.org/10.1016/j.triboint.2005.07.016>